



# Critical enhancement of the spin Hall effect by spin fluctuations



Satoshi Okamoto<sup>1</sup> ✉ & Naoto Nagaosa<sup>2</sup>

The spin Hall (SH) effect, the conversion of the electric current to the spin current along the transverse direction, relies on the relativistic spin-orbit coupling (SOC). Here, we develop a microscopic theory on the mechanisms of the SH effect in magnetic metals, where itinerant electrons are coupled with localized magnetic moments via the Hund exchange interaction and the SOC. Both antiferromagnetic metals and ferromagnetic metals are considered. It is shown that the SH conductivity can be significantly enhanced by the spin fluctuation when approaching the magnetic transition temperature of both cases. For antiferromagnetic metals, the pure SH effect appears in the entire temperature range, while for ferromagnetic metals, the pure SH effect is expected to be replaced by the anomalous Hall effect below the transition temperature. We discuss possible experimental realizations and the effect of the quantum criticality when the antiferromagnetic transition temperature is tuned to zero temperature.

The spin Hall (SH) effect<sup>1–3</sup> and its reciprocal effect, the inverse SH effect<sup>4</sup>, are among the most important components for the spintronic application<sup>5</sup> because they allow the electrical conversion between charge current and pure spin current, where electrons with opposite spin components flow along opposite directions with zero net charge current. Based on these effects, a variety of phenomena have been envisioned<sup>6,7</sup>. The SH effect and the anomalous Hall (AH) effect<sup>8</sup> are both rooted in the relativistic spin-orbit coupling (SOC), and these effects are traditionally understood as arising from intrinsic mechanisms, i.e., band effects<sup>9,10</sup>, or extrinsic mechanisms, i.e., impurity/disorder effects<sup>11–16</sup> and interfaces<sup>17</sup>.

There have appeared a number of proposals of the extrinsic mechanisms of the SH effect utilizing excitations or fluctuations in solids, such as phonons<sup>18–20</sup>. Identifying new mechanisms thus opens up a new research avenue and hereby helps to improve the efficiency of the SH effect, which remains small for practical applications<sup>21</sup>. Recently, the current authors proposed extrinsic mechanisms focusing on the spin fluctuation (SF) in nearly ferromagnetic (FM) disordered systems<sup>22</sup>. In these mechanisms, the critical SF associated with the zero-temperature FM quantum critical point (QCP) plays a fundamental role. It was predicted that the SH conductivity  $\sigma_{\text{SH}}$  is maximized at nonzero temperature when approaching the QCP. When the FM transition temperature  $T_C$  is finite, the pure SH effect is replaced by the AH effect below  $T_C$ , thus limiting the operation temperature range of the SH effect. This limitation could be lifted when the antiferromagnetic (AFM) SF is considered because the net magnetic moment is absent even below the AFM transition temperature  $T_N$ . From the study of

itinerant electron magnetism<sup>23</sup>, it has been recognized that the FM SF and the AFM SF provide qualitatively different behavior in electronic specific heat, conductivity, etc<sup>24–26</sup>. Thus, the SH effect could be another example that highlights the difference between FM SF and AFM SF.

While the SH effect due to the FM critical SF has not been experimentally examined, yet, refs. <sup>27–29</sup> examined the SH effect in FM alloys with finite  $T_C$ . In ref. <sup>27</sup>, Wei et al. reported that the temperature dependence of the inverse SH resistance of Ni-Pd alloys follows the uniform second-order nonlinear susceptibility  $\chi_2$ , but the inverse SH resistance has peaks above and below the Curie temperature and changes its sign at  $T_C$ . This behavior is consistent with the theoretical prediction in ref. <sup>30</sup>, which used a static mean field approximation to the model proposed by Kondo<sup>31</sup>. On the other hand in ref. <sup>28</sup>, Ou et al. reported that the inverse SH effect of Fe-Pt alloys is maximized near  $T_C$  as if it follows the uniform linear susceptibility. More recently, Wu et al. reported similar effects using Ni-Cu alloys<sup>29</sup>. For AFM systems, early work on Cr has already reported the large SH effects<sup>32,33</sup>. Recently, Fang and coworkers found that the SH conductivity in metallic Cr is enhanced when temperature is approaching the Néel temperature  $T_N$ <sup>34</sup>, suggesting the AFM SF as the main mechanism of the SH effect. However, the effect of AFM SF to the SH effect has not been theoretically addressed.

The main purpose of this work is to develop the theoretical description of the SH effect in magnetic metallic systems by the SF when the magnetic transition temperature ( $T_C$  or  $T_N$ ) is finite. Our theory is based on a microscopic model describing the coupling between itinerant electrons and localized magnetic moments by Kondo<sup>31</sup> and the self-consistent

<sup>1</sup>Materials Science and Technology Division, Oak Ridge National Laboratory, Oak Ridge, TN, USA. <sup>2</sup>RIKEN Center for Emergent Matter Science (CEMS), Wako, Saitama, Japan. ✉ e-mail: [okapon@ornl.gov](mailto:okapon@ornl.gov)

renormalization theory describing the fluctuation of localized moments by Moriya<sup>23</sup>. The main difference between AFM systems and FM systems is that the AFM ordering or correlation is characterized by the nonzero magnetic wave vector  $\mathbf{Q}$ . Thus, itinerant electrons scattered by the AFM SF gain or lose corresponding momentum. Our theory takes into account this momentum conservation appropriately. Despite this difference, it is demonstrated that the SH conductivity is enhanced as temperature is approaching  $T_C$  for FM systems or  $T_N$  for AFM systems. The result for the AFM systems strongly supports the conjecture made in ref.<sup>34</sup>. We highlight the qualitatively different behavior between the AFM SF and the FM SF near the finite-temperature phase transition and near the QCP.

For magnetic metallic systems, intrinsic mechanisms could also contribute to a variety of Hall effects, such as the AH effect by the Berry curvature and the topological Hall effect induced by chiral spin ordering. This work, however, does not cover these effects because these are band effects and do not show diverging behavior.

### Results

In this section, we present our main results. The first subsection is devoted to setting up our theoretical tools. We introduce the  $s$ - $d$  Hamiltonian, which is modified from the original form developed by Kondo<sup>31</sup>. Based on this model, the scattering mechanism for the SH conductivity will be clarified. Then, we set up the Gaussian action, which describes the SF based on the self-consistent renormalization theory by Moriya<sup>23</sup>. In the second subsection, theoretical results of the SH conductivity will be presented.

### Theoretical model and formalism

In this work, we consider three-dimensional systems. The  $s$ - $d$  Hamiltonian is written as  $H = H_0 + H_K$ . Here, the non-interacting itinerant electron part is described by  $H_0 = \sum_{\mathbf{k}, \nu} \epsilon_{\mathbf{k}} a_{\mathbf{k}\nu}^\dagger a_{\mathbf{k}\nu}$ , where  $\epsilon_{\mathbf{k}}$  is an energy eigenvalue at momentum  $\mathbf{k}$  given by  $\epsilon_{\mathbf{k}} = \frac{\hbar^2 k^2}{2m} - \epsilon_F$  with the Fermi energy  $\epsilon_F$  and the carrier effective mass  $m$ , and  $a_{\mathbf{k}\nu}^{(\dagger)}$  is an annihilation (creation) operator of an electron at momentum  $\mathbf{k}$  with the spin index  $\nu$ . We chose the simplest possible band structure as it allows detailed analytical calculations. This electronic part of the Hamiltonian is assumed to be unrenormalized<sup>23</sup>. However, as discussed briefly later, going beyond this assumption is necessary especially near the non-zero critical temperature. The  $s$ - $d$  coupling term in the original model has a mixed representation of momentum of conduction electrons and real-space coordinate of localized magnetic moments (see ref.<sup>31</sup> and Supplementary Note 1 for details). For magnetic metallic systems, where localized magnetic moments form a periodic lattice and conduction electrons hop through the same lattice sites, it is more convenient to express the model Hamiltonian entirely in the momentum space as

$$\begin{aligned}
 H_K = & -\frac{1}{\sqrt{N}} \sum_{\mathbf{k}, \mathbf{k}'} \sum_{\nu, \nu'} a_{\mathbf{k}\nu}^\dagger a_{\mathbf{k}'\nu'} [2(\mathbf{J}_{\mathbf{k}-\mathbf{k}'} \cdot \mathbf{s}_{\nu\nu'}) \\
 & \times \{\mathcal{F}_0 + 2\mathcal{F}_1(\mathbf{k} \cdot \mathbf{k}')\} + i\mathcal{F}_2 \mathbf{J}_{\mathbf{k}-\mathbf{k}'} \cdot (\mathbf{k}' \times \mathbf{k}) \\
 & + \frac{1}{\sqrt{N}} \sum_{\mathbf{p}} \mathcal{F}_3 \{(\mathbf{J}_{\mathbf{p}} \cdot \mathbf{s}_{\nu\nu'}) (\mathbf{J}_{\mathbf{k}-\mathbf{k}'-\mathbf{p}} \cdot (\mathbf{k}' \times \mathbf{k})) \\
 & + (\mathbf{J}_{\mathbf{p}} \cdot (\mathbf{k}' \times \mathbf{k})) (\mathbf{J}_{\mathbf{k}-\mathbf{k}'-\mathbf{p}} \cdot \mathbf{s}_{\nu\nu'}) \\
 & - \frac{2}{3} (\mathbf{J}_{\mathbf{p}} \cdot \mathbf{J}_{\mathbf{k}-\mathbf{k}'-\mathbf{p}}) (\mathbf{s}_{\nu\nu'} \cdot (\mathbf{k}' \times \mathbf{k}))\}].
 \end{aligned} \tag{1}$$

Here,  $\mathbf{s}_{\nu\nu'} = \frac{1}{2} \boldsymbol{\sigma}_{\nu\nu'}$  is the spin of a conduction electron with the Pauli matrices  $\boldsymbol{\sigma}$ .  $N$  is the total number of lattice sites.  $\mathbf{J}_{\mathbf{p}}$  is the Fourier transform of a local spin moment  $\mathbf{J}_n$  at position  $\mathbf{R}_n$  defined by  $\mathbf{J}_{\mathbf{p}} = \frac{1}{\sqrt{N}} \sum_n \mathbf{J}_n e^{-i\mathbf{p} \cdot \mathbf{R}_n}$ . Parameters  $\mathcal{F}_l$ <sup>22</sup> are related to  $F_l$  defined in ref.<sup>31</sup>.  $\mathcal{F}_{0,1}$  terms correspond to the standard  $s$ - $d$  exchange interaction or Hund coupling as depicted in Fig. 1a. Note that the  $\mathcal{F}_{0,1}$  terms represent ferromagnetic coupling. With these leading terms, the behavior of the theoretical model is less exotic than that with antiferromagnetic coupling often used in the context of heavy fermions<sup>35,36</sup>. The subleading  $\mathcal{F}_{2,3}$  terms represent the exchange of angular momentum between a conduction electron and a local moment. These terms are odd (linear or cubic)-order in  $\mathbf{J}_n$  and  $\mathbf{s}$  and induce the electron

deflection depending on the direction of  $\mathbf{J}_n$  or  $\mathbf{s}$ . More precisely, the  $\mathcal{F}_2$  term and the  $\mathcal{F}_3$  term generate the side-jump and the skew-scattering contributions to the SH conductivity, respectively, as depicted in Fig. 1b, c. From Eq. (1) and the position operator  $\mathbf{r}$ , the velocity operator is obtained as  $\mathbf{v} = (i/\hbar)[H_K, \mathbf{r}]$ . The anomalous velocity, the main source of the side-jump contribution, arises from the  $\mathcal{F}_2$  term (see Supplementary Note 1 for details).

From Eq. (1), one can notice the main difference from FM alloy systems<sup>22</sup>. Since itinerant electrons and localized moments share the same lattice structure, their coupling does not have a phase factor such as  $e^{i\mathbf{p} \cdot (\mathbf{R}_n - \mathbf{R}_{n'})}$ , where  $\mathbf{R}_n$  is the position of the localized moment  $\mathbf{J}_n$ . Therefore, the SF could contribute to the SH effect even if it has characteristic momentum  $\mathbf{Q} \neq \mathbf{0}$ , such as in AFM systems, without introducing destructive effects. Otherwise, averaging over the lattice coordinate would lead to zero SH effect as  $\langle e^{i\mathbf{Q} \cdot (\mathbf{R}_n - \mathbf{R}_{n'})} \rangle \approx 0$ .

To describe the fluctuation of localized moments  $\mathbf{J}_n$ , we adopt a generic Gaussian action given by<sup>23,37-40</sup>,

$$A_{\text{Gauss}} = \frac{1}{2} \sum_{\mathbf{p}, l} D_{\mathbf{p}}^{-1}(i\omega_l) \mathbf{J}_{\mathbf{p}}(i\omega_l) \cdot \mathbf{J}_{-\mathbf{p}}(-i\omega_l) \tag{2}$$

with

$$D_{\mathbf{p}}(i\omega_l) = \frac{1}{\delta + A|\mathbf{p} - \mathbf{Q}|^2 + |\omega_l|/\Gamma_{\mathbf{p}}}. \tag{3}$$

Here,  $\mathbf{J}_{\mathbf{p}}(i\omega_l)$  is a space and imaginary-time  $\tau$  Fourier transform of  $\mathbf{J}_n(\tau)$ , where we made the  $\tau$  dependence explicit, and  $\omega_l = 2l\pi T$  is the bosonic Matsubara frequency. Parameter  $A$  is introduced as a constant so that  $A|\mathbf{p} - \mathbf{Q}|^2$  has the unit of energy, and  $\delta$  is the distance from the magnetic transition temperature and is related to the magnetic correlation length as  $\xi \propto \delta^{-1/2}$  at  $T > T_{N,C}$  and to the ordered magnetic moment as  $M(T) \propto \delta^{1/2}$  at  $T < T_{N,C}$ .  $\Gamma_{\mathbf{p}}$  represents the Landau damping, whose momentum dependence is neglected for AFM systems,  $\Gamma_{\mathbf{p}} = \Gamma$ , since it is weak near the magnetic wave vector  $\mathbf{Q}$ . For FM systems with  $\mathbf{Q} = \mathbf{0}$ , the damping term has a momentum dependence as  $\Gamma_{\mathbf{p}} = \Gamma p$ . With impurity scattering or disorder,  $\Gamma_{\mathbf{p}}$  remains finite below a cutoff momentum  $|\mathbf{p}| \leq q_c$  as  $\Gamma_{\mathbf{p}} = \Gamma q_c$ .

While the above Gaussian action can be derived by solving an interacting electron model, it is a highly nontrivial problem and dependent on the detail of theoretical model and the target material. Instead, we adopt a conventional approach, where the material dependence is described by a small number of parameters and derive the spin Hall conductivity arising from the spin fluctuation and the subleading terms of Eq. (1). In fact, theoretical analyses based on this Gaussian action have been successful to

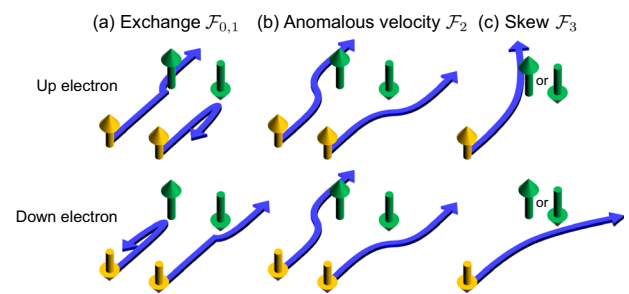


**Fig. 1 | Schematic view of the Kondo model.** **a** Spin dependent scattering by  $\mathcal{F}_{0,1}$  terms, **b** anomalous velocity induced by  $\mathcal{F}_2$  terms, and **c** skew scattering by  $\mathcal{F}_3$  terms. Yellow arrows indicate conduction electrons, and green arrows indicate local moments. In the  $\mathcal{F}_{2(3)}$  scattering processes, the electron deflection depends on the direction of the local moment (the electron spin), leading to the side-jump (skew-scattering) contribution to  $\sigma_{\text{SH}}$ . Adapted from Okamoto, S., Egami, T. & Nagaosa, N. Phys. Rev. Lett. **123**, 196603 (2019).

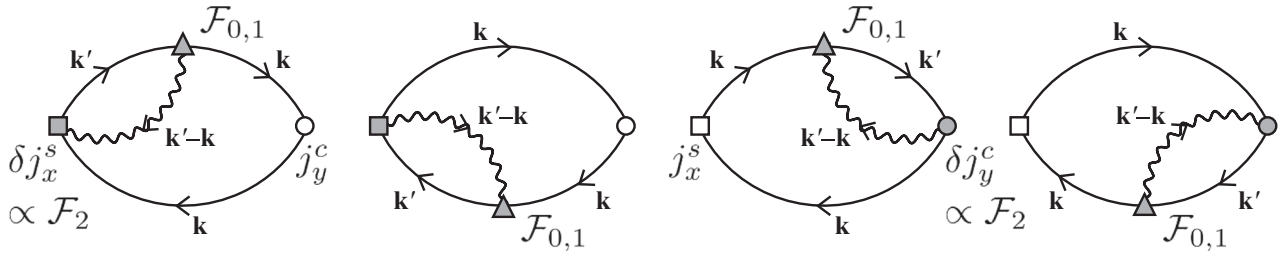


**Fig. 2 | Diagrammatic representation for the side-jump contribution.** Solid (wavy) lines are the electron Green's functions (the SF propagators). Squares (circles) are the spin (charge) current vertices, with filled symbols representing the

velocity correction with  $\mathcal{F}_2$ , i.e., side jump. Filled triangles are the interaction vertices with  $\mathcal{F}_{0,1}$ . Adapted from Okamoto, S., Egami, T. & Nagaosa, N. *Phys. Rev. Lett.* **123**, 196603 (2019).

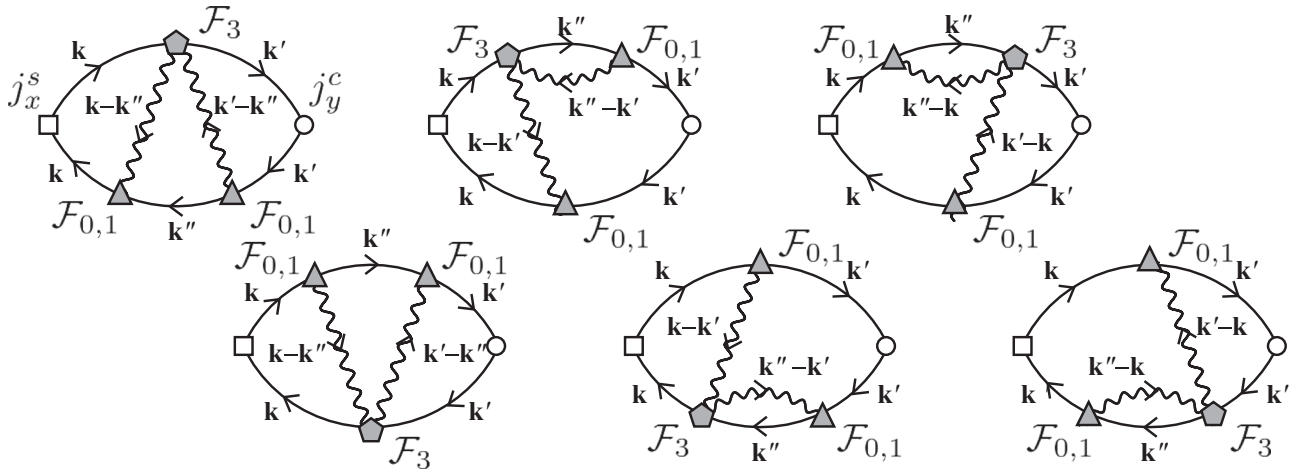


**Fig. 3 | Diagrammatic representation for the skew-scattering contribution.** Filled pentagons are the interaction vertices with  $\mathcal{F}_3$ . The definitions of the other symbols or lines are the same as in Fig. 2. Adapted from Okamoto, S., Egami, T. & Nagaosa, N. *Phys. Rev. Lett.* **123**, 196603 (2019).

explain many experimental results on itinerant magnets<sup>23</sup>. In principle,  $\delta$  depends on temperature and is determined by solving self-consistent equations for a full model including non-Gaussian terms<sup>23,37–41</sup>. However, the temperature dependence of  $\delta$  is known for the following three cases in three dimension. I:  $\delta \propto T - T_{N,C}$  at  $T \gtrsim T_{N,C}$ . II:  $\delta \propto M^2(T) \propto T_{N,C} - T$  at  $T \lesssim T_{N,C}$  and III:  $\delta \propto T^{3/2}$  at  $T \sim 0$  when  $T_N \rightarrow 0$ , i.e., approaching the QCP. For FM with impurity scattering or disorder  $\delta \propto T^{3/2}$  at  $T \sim 0$  when  $T_C \rightarrow 0$ , while for clean FM  $\delta \propto T^{4/3}$ .

**Spin-Hall conductivity**

With the above preparations, we analyze the SH conductivity using the Matsubara formalism, by which one can take the dynamical SF into account via a diagrammatic technique. Here, the frequency-dependent SH conductivity is considered as  $\sigma_{SH}(i\Omega_l)$ .  $\Omega_l$  is the bosonic Matsubara frequency, which is analytically continued to real frequency as  $i\Omega_l \rightarrow \Omega + i0^+$  at the end of the analysis, and then the DC limit,  $\Omega \rightarrow 0$ , is taken to obtain  $\sigma_{SH}$ . Based on the diagrammatic representations in Figs. 2 and 3,  $\sigma_{SH}$  is expressed in terms of electron Green's function  $G$  and the propagator  $D$  of the longitudinal SF. While the transverse SFs or spin wave excitations exist below the magnetic transition temperature, the scattering of electrons by such SFs does not show a critical behavior<sup>42,43</sup>, and its contribution is expected to be small. Therefore, for our analysis, we consider only longitudinal SFs below  $T_{N,C}$ .

We first focus on the SH effect by the AFM SF. By carrying out the Matsubara summations, the energy integrals and the momentum summations as detailed in Supplementary Note 2, we find

$$\sigma_{AFM,SH}^{side\ jump} \approx \frac{e^2 m \tau_{\mathbf{k}}}{2\pi^3 \hbar^4 |\mathbf{Q}|} A_{AFM}^{side\ jump} \tilde{I}_{AFM}(T, \delta) \tag{4}$$

for the side-jump contribution and

$$\sigma_{AFM,SH}^{skew\ scatt.} \approx \frac{e^2 \tau_{\mathbf{k}}^2 \Gamma \delta}{2\pi^2 \hbar^3 |\mathbf{Q}|} A_{AFM}^{skew\ scatt.} I_{AFM}^2(T, \delta) \tag{5}$$

for the skew-scattering contribution. Here,  $e$  is the elementary charge. In both cases,  $\tau_{\mathbf{k}}$  is the carrier lifetime on the Fermi surface at special momenta  $\mathbf{k}$  that satisfies the nesting condition. Such momenta  $\mathbf{k}$  form loops on the Fermi surface. With the parabolic band, the carrier lifetime due to the AFM SF along such loops is independent of momentum as detailed in Supplementary Note 4. The momentum dependence of the carrier lifetime due to other effects, such as disorder and phonons, is weak. Thus, we assume that  $\tau_{\mathbf{k}}$  is a constant. The functions  $\tilde{I}_{AFM}(T, \delta)$  and  $I_{AFM}(T, \delta)$  defined in Supplementary Note 2 represent the coupling between conduction electrons and the dynamical SF.  $A_{AFM}^{side\ jump}$  and  $A_{AFM}^{skew\ scatt.}$  are constants defined by the integrals over the azimuth angle of momentum  $\mathbf{k}$  measured from the direction of  $\mathbf{Q}$  as described in Supplementary Note 2. Since the angle integrals give only geometrical factors of  $\mathcal{O}(1)$ ,  $A_{AFM}^{side\ jump} \approx \mathcal{F}_0 \mathcal{F}_2 k_F^2$  and  $A_{AFM}^{skew\ scatt.} \approx \mathcal{F}_0^2 \mathcal{F}_3 k_F^4$ .

Similarly, the SH conductivity due to the FM SF is obtained (for details, see Supplementary Note 3) as

$$\sigma_{FM,SH}^{side\ jump} \approx \frac{2e^2 \tau_{\mathbf{k}}}{m} A_{FM}^{side\ jump} I_{FM}(T, \delta) \tag{6}$$

for the side-jump contribution and

$$\sigma_{FM,SH}^{skew\ scatt.} \approx \frac{4e^2 \hbar \tau_{\mathbf{k}}^2}{m^2} A_{FM}^{skew\ scatt.} I_{FM}^2(T, \delta) \tag{7}$$

**Table 1 |  $T$  dependence of  $\sigma_{SH}$**

$T$ regime	$\sigma_{AFM,SH}^{side\ jump}$	$\sigma_{AFM,SH}^{skew\ scatt.}$	$\sigma_{FM,SH}^{side\ jump}$	$\sigma_{FM,SH}^{skew\ scatt.}$
I $T > T_{N,C}$	$\propto \tau_k T^2 / \sqrt{T - T_N}$	$\propto \tau_k^2 T^6 / (T - T_N)$	$\propto \tau_k T^3 / (T - T_C)$	$\propto \tau_k^2 T^6 / (T - T_C)^2$
II $T < T_{N,C}$	$\propto \tau_k T^2 / \sqrt{T_N - T}$	$\propto \tau_k^2 T^6 / (T_N - T)$	$\propto \tau_k T^3 / (T_C - T)$	$\propto \tau_k^2 T^6 / (T_C - T)^2$
III $T \sim 0 (T_{N,C} \rightarrow 0)$	$\propto \tau_k T^{3/2}$	$\propto \tau_k^2 T^{9/2}$	$\propto \tau_k T^{3/2a}$	$\propto \tau_k^2 T^{3b}$

An additional  $T$  dependence appears via the carrier lifetime  $\tau_k$ . Note that the scaling law breaks down in the vicinity of the transition temperature  $T_{N,C}$  as indicated by shades in Figs. 4 and 5. See the main text for details.

<sup>a</sup> In the absence of disorder or impurity scattering, this temperature dependence is modified as  $\propto \tau_k T^{5/3}$ .

<sup>b</sup> In the absence of disorder or impurity scattering, this temperature dependence is modified as  $\propto \tau_k^2 T^{10/3}$ .

§ Not considered in the main text, but briefly discussed in Supplementary Note 5.

for the skew-scattering contribution. Here,  $\tau_k$  is the carrier lifetime on the Fermi surface, and the constants  $A_{FM}^{side\ jump}$  and  $A_{FM}^{skew\ scatt.}$  are given by  $A_{FM}^{side\ jump} \approx \frac{mk_F^3}{\pi^2 \hbar} \mathcal{F}_0 \mathcal{F}_2$  and  $A_{FM}^{skew\ scatt.} \approx \frac{mk_F^5}{\pi^2 \hbar} \mathcal{F}_0^2 \mathcal{F}_3$ , respectively. The function  $I_{FM}(T, \delta)$  is defined in Supplementary Note 3.

### Temperature dependence of the Spin-Hall conductivity

Reflecting the temperature dependence of spin dynamics,  $\sigma_{SH}$  by the SF could show a strong temperature dependence. This is governed by the functions  $\tilde{I}_{AFM}(T, \delta)$ ,  $I_{AFM}(T, \delta)$ , and  $I_{FM}(T, \delta)$ , and the carrier lifetime  $\tau_k$ .  $\tau_k$  has several contributions, such as the disorder or impurity effects  $\tau_{dis}$ , which  $T$  dependence is expected to be small, the electron-electron interactions  $\tau_{ee}$ , the electron-phonon interactions  $\tau_{ep}$ , and the scattering due to the SF  $\tau_{sf}$ . Within the current model,  $\tau_{sf} \approx \frac{\hbar}{2} \mathcal{F}_0^{-2} I_{AFM,FM}^{-1}(T, \delta)$  (see Supplementary Note 4 for details).

In addition to the different momentum dependencies in the damping term  $\Gamma_p$ , the AFM SF and the FM SF have fundamentally different characters due to the momentum conservation during scattering events. For the AFM case, electrons scattered by the SF gain or lose momentum  $\mathbf{Q}$ . As a result,  $\sigma_{AFM,SH}^{skew\ scatt.}$  in Eq. (5) has extra  $\delta$  [for comparison, see Eq. (7)]. Furthermore,  $\sigma_{AFM,SH}^{side\ jump}$  has  $\tilde{I}_{AFM}(\delta, T)$ , whose temperature dependence somewhat differs from  $I_{AFM}(\delta, T)$ .  $\tilde{I}_{AFM}(\delta, T)$  has the same temperature dependence of the scattering rate due to the AFM SF as reported by ref. <sup>43</sup>. While the result of ref. <sup>43</sup> was obtained by loosening the momentum conservation by averaging the electron self-energy over the Fermi surface, the momentum dependence is explicitly considered in our  $\sigma_{AFM,SH}^{side\ jump}$ . These differences in the scattering process lead to the different temperature dependence in  $\sigma_{SH}$  by the AFM SF and the FM SF.

Supplementary Table I summarizes the  $T$  dependence of  $\delta$  and  $T$ - $\delta$  dependence of  $\tilde{I}_{AFM}(T, \delta)$ ,  $I_{AFM}(T, \delta)$ , and  $I_{FM}(T, \delta)$  in three  $T$  regimes I–III and in the vicinity of the magnetic phase transition at  $T_{N,C}$  between regimes I and II. By including the  $T$  dependence of  $\delta$ , the full  $T$  dependence of  $\tilde{I}_{AFM}(T, \delta)$  and  $I_{AFM,FM}(T, \delta)$  is fixed as follows: In the regimes I and II,  $\tilde{I}_{AFM}(T, \delta)$ ,  $I_{AFM}(T, \delta)$ , and  $I_{FM}(T, \delta)$  are enhanced as  $T \rightarrow T_{N,C}$  as  $\tilde{I}_{AFM}(T, \delta) \propto \delta^{-1/2} \propto 1/\sqrt{|T - T_N|}$ ,  $I_{AFM}(T, \delta) \propto \delta^{-1} \propto 1/|T - T_N|$ , and  $I_{FM}(T, \delta) \propto \delta^{-1} \propto 1/|T - T_C|$ , respectively. While the divergence of  $\tilde{I}_{AFM}(T, \delta)$  is cutoff at  $T_N$ , the  $1/|T - T_{N,C}|$  divergence of  $I_{AFM,FM}(T, \delta)$  at  $T_{N,C}$  is weakened to the logarithmic divergence  $-\ln|T - T_N|$  or the smaller power  $1/\sqrt{|T - T_C|}$ . Note however that this behavior of  $I_{AFM,FM}(T, \delta)$  right at  $T_{N,C}$  is a result of the current treatment which does not include the feedback between the carrier lifetime and the SF spectrum. We anticipate that including such feedback effects will cutoff these divergences. Since this requires one to solve the full Hamiltonian, including electron-electron interactions self-consistently, such a treatment is left for the future study. The SH angle  $\Theta_{SH} = \sigma_{SH}/\sigma_c$ , where  $\sigma_c$  is the charge conductivity, is expected to be much smaller than 1, even though  $\Theta_{SH}$  could be enhanced at the critical temperature, because  $\sigma_{SH}$  and  $\sigma_c$  are both proportional to the carrier lifetime. On the other hand, the behavior near the QCP, the regime III, is qualitatively reliable. This is because, the scattering rate  $\tau_k^{-1}$  for the pure case and  $I_{AFM,FM}(T, \delta)$  approach 0 with  $T \rightarrow 0$  and, and fulfill the self-consistency condition between them. In this regime, however,  $\tau_k$  diverges with  $T \rightarrow 0$  without disorder effects. This could leads to the pathological

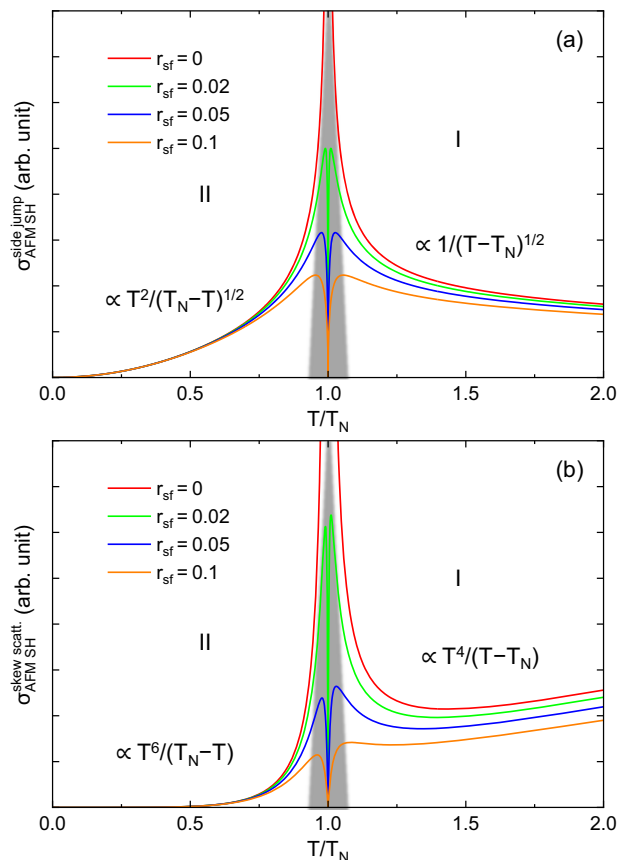


**Fig. 4 | Schematic temperature dependence of the SH conductivity of anti-ferromagnets in the  $T$  regimes I and II with nonzero  $T_N$ .** The side-jump contribution  $\sigma_{AFM,SH}^{side\ jump}$  is shown in **a** and the skew-scattering contribution  $\sigma_{AFM,SH}^{skew\ scatt.}$  is shown in **b**. The carrier lifetime is modeled as  $\tau_k^{-1} = r_{dis} + r_{ee} T^2 + r_{sf} T^3 / |T - T_N|$ , with  $r_{dis}$ ,  $r_{ee}$ , and  $r_{sf}$  terms representing the disorder and impurity effects, electron-electron interaction, and the AFM SF, respectively.  $r_{sf}$  is varied with fixing  $r_{dis} = r_{ee} = 1$ . Shaded areas indicate where the current treatment breaks down, requiring the self-consistent treatment.

divergence of  $\sigma_{SH}$ . We will not consider such a situation in the main text, and give a brief discussion in Supplementary Note 5.

The temperature dependence of  $\sigma_{SH}$  coming from  $\delta$ ,  $\tilde{I}_{AFM}$ , and  $I_{AFM,FM}$  is summarized in Table 1. Reflecting the diverging behavior of  $\tilde{I}_{AFM}$  and  $I_{AFM,FM}$ ,  $\sigma_{SH}$  is sharply enhanced as  $T \rightarrow T_{N,C}$  in the regimes I and II, as displayed in Fig. 4 for the AFM case and Fig. 5 for the FM case. Here, the approximate inverse carrier lifetime appropriate in these  $T$  regimes is considered as  $\tau_k^{-1} = r_{dis} + r_{ee} T^2 + r_{sf} T^3 / |T - T_{N,C}|$ , where  $r_{dis}$ ,  $r_{ee}$ , and  $r_{sf}$  terms correspond to the disorder effect, electron-electron interaction<sup>44</sup>, and the SF, respectively. Focusing on the low  $T$  behavior, we ignored the electron-phonon coupling, which would contribute to the carrier lifetime at

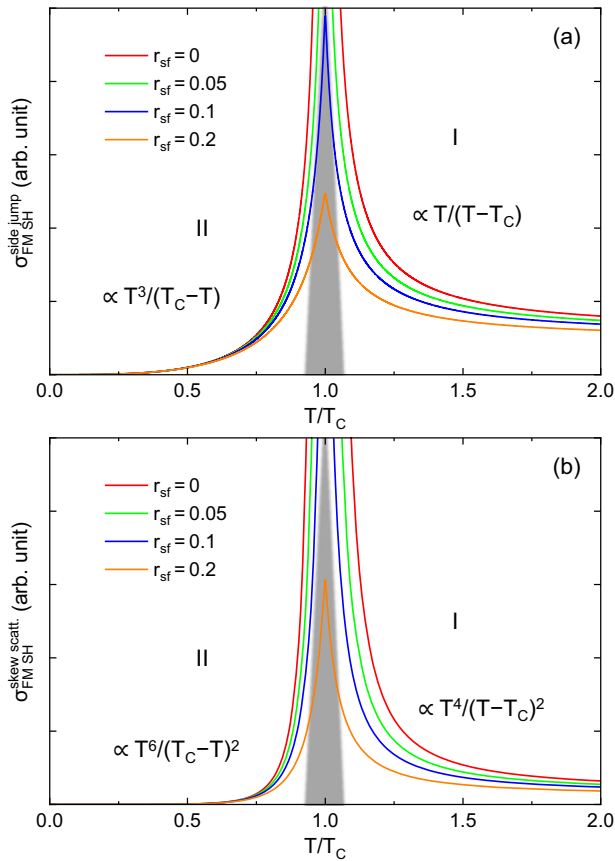


**Fig. 5 | Schematic temperature dependence of the SH conductivity ferromagnets in the  $T$  regimes I and II with nonzero  $T_C$ .** The side-jump contribution  $\sigma_{\text{FM,SH}}^{\text{side jump}}$  is shown in **a** and the skew-scattering contribution  $\sigma_{\text{FM,SH}}^{\text{skew scatt.}}$  is shown in **b**. The carrier lifetime is modeled as  $\tau_k^{-1} = r_{\text{dis}} + r_{\text{ee}} T^2 + r_{\text{sf}} T^3 / |T - T_C|$ , with  $r_{\text{dis}}$ ,  $r_{\text{ee}}$ , and  $r_{\text{sf}}$  terms representing the disorder and impurity effects, electron-electron interaction, and the FM SF, respectively.  $r_{\text{sf}}$  is varied with fixing  $r_{\text{dis}} = r_{\text{ee}} = 1$ . Shaded areas indicate where the current treatment breaks down, requiring the self-consistent treatment.

high temperatures close to the Debye temperature<sup>45,46</sup>. In the current theory, there are three energy units; the Fermi energy  $\epsilon_F \approx \hbar v_F / a$ , the spin stiffness  $A / a^2$  and magnetic transition temperature  $T_{N,C}$ . The temperature dependence of  $\sigma_{\text{AFM,SH}}^{\text{skew scatt.}}$  and  $\sigma_{\text{FM,SH}}^{\text{side jump}}$  is from  $I_{\text{AFM,FM}}(T, \delta)$ , and therefore  $T$  is scaled by  $\epsilon_F$ , while  $\sigma_{\text{AFM,SH}}^{\text{side jump}}$  is from  $\tilde{I}_{\text{AFM}}(T, \delta)$  and  $T$  is scaled by  $A / a^2$ . For the analytical plots, we use the dimensionless unit for temperature, where  $T$  is scaled by these energy units, and  $T_{N,C} = 1$  for the  $T$  regimes I and II. With this convention,  $r_{\text{dis}}$ ,  $r_{\text{ee}}$ ,  $r_{\text{sf}}$  have the unit of inverse time.

Despite the diverging trend as  $T \rightarrow T_N$ ,  $\sigma_{\text{AFM,SH}}^{\text{side jump}}$  and  $\sigma_{\text{AFM,SH}}^{\text{skew scatt.}}$  sharply drop to zero in the vicinity of  $T_N$  with nonzero  $r_{\text{sf}}$ . This is caused by the suppression of  $\tau_k$  due to the SF as  $\tau_k \approx r_{\text{sf}}^{-1} |T - T_N| / T^3$ . We anticipate that a self-consistent treatment of the original interacting electron model kills this entire suppression, leading to a smooth  $T$  dependence of  $\sigma_{\text{SH}}$ .

$\sigma_{\text{FM,SH}}^{\text{side jump}}$  and  $\sigma_{\text{FM,SH}}^{\text{skew scatt.}}$  have stronger  $T$  dependence than the AFM counterparts, leading to the divergence with  $T$  approaches  $T_C$  with  $r_{\text{sf}} = 0$ . Nonzero  $r_{\text{sf}}$  suppresses the divergence in  $\sigma_{\text{FM,SH}}^{\text{side jump}}$  and  $\sigma_{\text{FM,SH}}^{\text{skew scatt.}}$  in the vicinity of  $T_C$ , leading to sharp cusps. However, similar to the AFM case, we anticipate that a self-consistent treatment of the original model leads to a smooth  $T$  dependence of  $\sigma_{\text{SH}}$  across  $T_C$ .

Because of the competition between the divergence of  $I_{\text{AFM,FM}}(T, \delta)$  and the suppression of  $\tau_k$ , it might be challenging to deduce the precise temperature scaling of the SH conductivity at  $T_{N,C}$ . Nevertheless, our result summarized in Table 1 will be helpful to analyze experimental SH conductivity because the two contributions are separated.

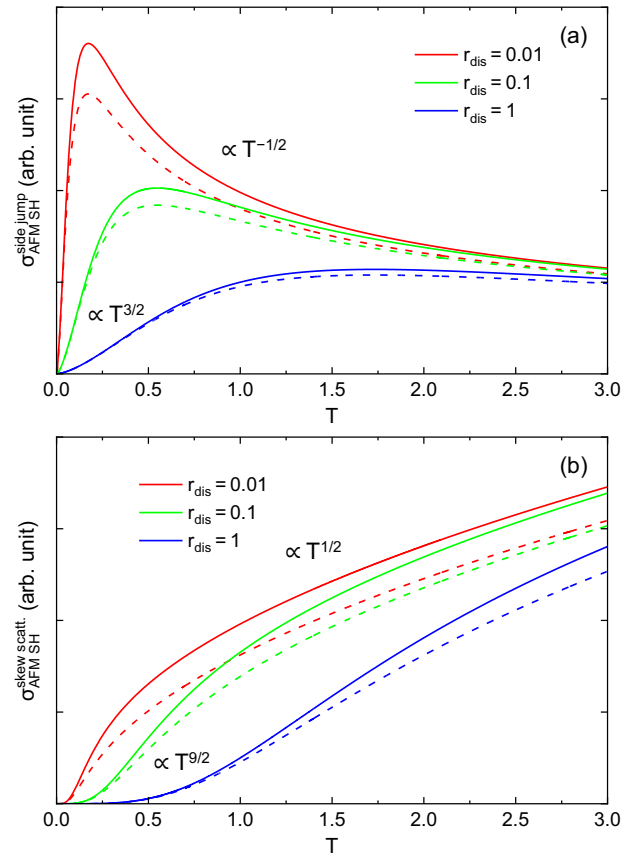


**Fig. 6 | Schematic temperature dependence of the SH conductivity of anti-ferromagnets in the  $T$  regime III with  $T_N > 0$ .** The side-jump contribution  $\sigma_{\text{AFM,SH}}^{\text{side jump}}$  is shown in **a**, and the skew-scattering contribution  $\sigma_{\text{AFM,SH}}^{\text{skew scatt.}}$  is shown in **b**. The carrier lifetime is modeled as  $\tau_k^{-1} = r_{\text{dis}} + r_{\text{ee}} T^2 + r_{\text{sf}} T^{3/2}$ , and  $r_{\text{dis}}$  is varied with fixing  $r_{\text{ee}} = 1$  and  $r_{\text{sf}} = 0.0(0.1)$  for solid (dashed) lines.

For the quantum critical regime III, the carrier lifetime has the temperature dependence as  $\tau_k^{-1} = r_{\text{dis}} + r_{\text{ee}} T^2 + r_{\text{sf}} T^{3/2}$  for the AFM case and the FM with disorder effects. The temperature dependence of  $\sigma_{\text{SH}}$  is strongly influenced by that of  $\tau_k$ . Thus, here we discuss the cases with disorder effect which make  $\tau_k$  finite at  $T = 0$ . Special cases, where the disorder effect is absent and  $\tau_k$  becomes infinity at  $T = 0$ , will be briefly discussed in Supplementary Note 5.

The schematic temperature dependence of  $\sigma_{\text{AFM,SH}}$  and  $\sigma_{\text{FM,SH}}$  is shown in Figs. 6 and 7, respectively. With nonzero  $r_{\text{dis}}$ , all  $\sigma_{\text{SH}}$  approach 0 with  $T$  goes to 0 but with different  $T$  scaling:  $\sigma_{\text{AFM,SH}}^{\text{side jump}} \propto T^{3/2}$ ,  $\sigma_{\text{AFM,SH}}^{\text{skew scatt.}} \propto T^{9/2}$ ,  $\sigma_{\text{FM,SH}}^{\text{side jump}} \propto T^{3/2}$ , and  $\sigma_{\text{FM,SH}}^{\text{skew scatt.}} \propto T^3$ . For the latter two cases, different power laws of  $T$  were predicted in ref. 22 as described in Supplementary Note 3.

Interestingly,  $\sigma_{\text{AFM,SH}}^{\text{side jump}}$  and  $\sigma_{\text{FM,SH}}^{\text{side jump}}$  show formally the same leading  $T$  dependence because the divergence of the SF propagator has a cutoff by  $|\mathbf{Q}|$  in the former and  $q_c$  in the latter. On the other hand,  $\sigma_{\text{AFM,SH}}^{\text{skew scatt.}}$  and  $\sigma_{\text{FM,SH}}^{\text{skew scatt.}}$  show contrasting  $T$  dependence; the former continuously decreases with decreasing  $T$  while the latter first increases, shows maximum, and finally goes to zero with decreasing  $T$  because of the competition between  $\tau_k$  and  $I_{\text{FM}}(T, \delta)$ .

## Discussion

We have seen that the SH effect in magnetic metallic systems induced by spin fluctuations has different contributions with different temperature scaling. In this section, we consider remaining questions regarding the relative strength between different contributions as well as the experimental/materials realization of our theory.

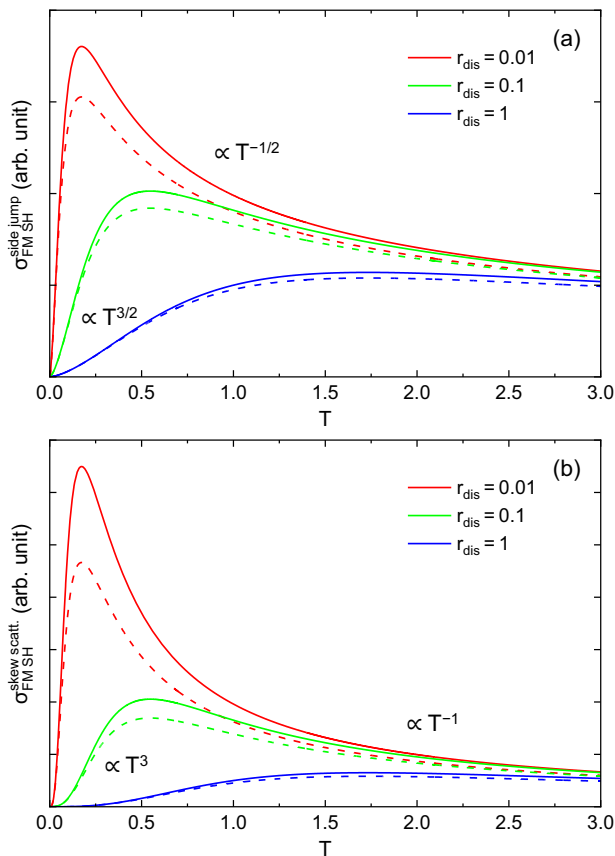


**Fig. 7 | Schematic temperature dependence of the SH conductivity of ferromagnets in the  $T$  regime III with  $T_C > 0$ .** The side-jump contribution  $\sigma_{\text{AFM,SH}}^{\text{side jump}}$  is shown in (a), and the skew-scattering contribution  $\sigma_{\text{AFM,SH}}^{\text{skew scatt.}}$  shown in (b). The carrier lifetime is modeled as  $\tau_{\mathbf{k}}^{-1} = r_{\text{dis}} + r_{\text{ee}}T^2 + r_{\text{sf}}T^{3/2}$ , and  $r_{\text{dis}}$  is varied with fixing  $r_{\text{ee}} = 1$  and  $r_{\text{sf}} = 0(0.1)$  for solid (dashed) lines.

When the FM critical fluctuation is dominant in the carrier lifetime in the temperature regime III, the carrier lifetime is given by  $\tau_{\text{sf}} \approx \hbar/2\{F_0 + 2F_1k_{\text{F}}^2\}I_{\text{FM}}(T, \delta)$ , and therefore the ratio between the maximum  $\sigma_{\text{AFM,SH}}^{\text{skew scatt.}}$  and the maximum  $\sigma_{\text{AFM,SH}}^{\text{side jump}}$  is estimated as  $\sigma_{\text{AFM,SH}}^{\text{skew scatt.}}/\sigma_{\text{AFM,SH}}^{\text{side jump}} \approx \varepsilon_{\text{F}}\mathcal{F}_3/\mathcal{F}_0\mathcal{F}_2$  (see, Eqs. (6) and (7) and the discussion in ref. 22). From the typical interaction strengths  $\mathcal{F}$ s and the Fermi energy  $\varepsilon_{\text{F}}$ , the maximum of  $\sigma_{\text{AFM,SH}}^{\text{skew scatt.}}$  is expected to be 1 to 2 orders of magnitude larger than that of  $\sigma_{\text{AFM,SH}}^{\text{side jump}}$ . This relation is expected to hold for the FM case with finite  $T_C$ .

When disorder effects or electron-electron scattering becomes dominant in the carrier lifetime, the magnitude of  $\tau_{\mathbf{k}}$  and  $I_{\text{FM}}(T, \delta)$  has to be explicitly considered. Using the asymptotic form of  $I_{\text{FM}}(T, \delta)$  near  $\delta \sim 0$  in the  $T$  regimes of I, II, and III,  $I_{\text{FM}}(T, \delta) \approx \frac{1}{8\pi} \left(\frac{aT}{\hbar v_{\text{F}}}\right)^3 \frac{1}{\delta}$  (see Supplementary Note 3 for details) the ratio between  $\sigma_{\text{AFM,SH}}^{\text{skew scatt.}}$  and  $\sigma_{\text{AFM,SH}}^{\text{side jump}}$  is estimated as

$$\frac{\sigma_{\text{AFM,SH}}^{\text{skew scatt.}}}{\sigma_{\text{AFM,SH}}^{\text{side jump}}} \approx \frac{k_{\text{F}}^2}{4\pi m} \tau_{\mathbf{k}} \mathcal{F}_0 \frac{\mathcal{F}_3}{\mathcal{F}_2} \left(\frac{aT}{\hbar v_{\text{F}}}\right)^3 \frac{1}{\delta}. \quad (8)$$

Because of the factor of  $1/\delta$ , this ratio diverges when  $\delta$  goes to zero as  $T$  approaches  $T_C$  as long as  $\tau_{\mathbf{k}}$  is finite. Thus, the skew-scattering mechanism is expected to become dominant near the critical temperature. On the other hand near the FM QCP, the side-jump contribution may grow with lowering temperature when the carrier lifetime is dominated by other mechanisms than the SF.

In the AFM-fluctuation case, the situation is more complicated. This is because the side-jump contribution and the skew-scattering contribution have different temperature dependence,  $\tilde{I}_{\text{AFM}}(T, \delta)$  vs.  $I_{\text{AFM}}(T, \delta)$ , while they show similar enhancement near the magnetic transition temperature. Therefore, the microscopic parameters determining the SF come into play. To see this, first consider the temperature regimes I and II, where the leading temperature dependence of  $\sigma_{\text{AFM,SH}}^{\text{side jump}}$  and  $\sigma_{\text{AFM,SH}}^{\text{skew scatt.}}$  is given by

$$\sigma_{\text{AFM,SH}}^{\text{side jump}} \approx \frac{e^2 m}{32\pi^2 \hbar^4} \frac{\tau_{\mathbf{k}}}{|\mathbf{Q}|} \mathcal{F}_0 k_{\text{F}}^2 \mathcal{F}_2 \frac{T^2}{\Gamma \sqrt{\delta(A/a^2)^3}} \quad (9)$$

and

$$\sigma_{\text{AFM,SH}}^{\text{skew scatt.}} \approx \frac{e^2}{128\pi^3 \hbar^3} \frac{\tau_{\mathbf{k}}^2}{|\mathbf{Q}|} \mathcal{F}_0^2 k_{\text{F}}^2 \mathcal{F}_3 \left(\frac{T}{\varepsilon_{\text{F}}}\right)^6 \frac{\Gamma}{\delta}, \quad (10)$$

respectively. Here, we approximate  $k_{\text{F}} \approx 1/a$  (inverse lattice constant), so that  $\hbar v_{\text{F}}/a \approx \varepsilon_{\text{F}}$ . The ratio between these two contributions leads to

$$\frac{\sigma_{\text{AFM,SH}}^{\text{skew scatt.}}}{\sigma_{\text{AFM,SH}}^{\text{side jump}}} \approx \frac{1}{2\pi} \frac{\tau_{\mathbf{k}}}{\hbar} \Gamma^2 \mathcal{F}_0 \frac{\mathcal{F}_3}{\mathcal{F}_2} \frac{T^4}{\varepsilon_{\text{F}}^5} \sqrt{\frac{(A/a^2)^3}{\delta}}. \quad (11)$$

Thus, the relative strength depends on both electronic properties and the SF. On the electronic part, (i) longer lifetime  $\tau_{\mathbf{k}}$ , (ii) larger  $\mathcal{F}_3$  than  $\mathcal{F}_2$ , and (iii) smaller Fermi energy  $\varepsilon_{\text{F}}$  prefer the skew-scattering mechanism over the side jump. On the SF part, (iv) larger  $A$ , corresponding to spin stiffness or magnetic exchange, (v) larger damping ratio  $\Gamma$ , which is a dimensionless parameter here but is proportional to the electron density of states at the Fermi level, and (vi) smaller  $\delta$  prefer the skew-scattering contribution.

Near the AFM QCP (the  $T$  regime III),  $\sigma_{\text{AFM,SH}}^{\text{side jump}}$  is modified as

$$\sigma_{\text{AFM,SH}}^{\text{side jump}} \approx \frac{e^2 m}{2\pi^3 \hbar^4} \frac{\tau_{\mathbf{k}}}{|\mathbf{Q}|} \mathcal{F}_0 k_{\text{F}}^2 \mathcal{F}_2 \frac{T^{3/2}}{\Gamma \sqrt{(A/a^2)^3}}. \quad (12)$$

Hence, with  $\delta = T^{3/2}$ , the ratio between the two contributions becomes

$$\frac{\sigma_{\text{AFM,SH}}^{\text{skew scatt.}}}{\sigma_{\text{AFM,SH}}^{\text{side jump}}} \approx \frac{\pi}{32} \frac{\tau_{\mathbf{k}}}{\hbar} \Gamma^2 \mathcal{F}_0 \frac{\mathcal{F}_3}{\mathcal{F}_2} \frac{T^3}{\varepsilon_{\text{F}}^5} \sqrt{(A/a^2)^3}. \quad (13)$$

Thus,  $\sigma_{\text{AFM,SH}}^{\text{side jump}}$  is expected to become progressively dominant as  $T \rightarrow 0$ . This could be seen in the contrasting  $T$  dependence of  $\sigma_{\text{AFM,SH}}$  as plotted in Fig. 6.

In this work, we first considered the SH effect by the AFM SF, which is relevant to AFM metallic Cr. As early studies have reported, metallic Cr shows large SH effect<sup>32,33</sup>. With the small SOC for a  $3d$  element, this indicates additional contributions to the SH effect. Recent study used high-quality single crystal of Cr and revealed the detailed temperature dependence of the SH conductivity<sup>34</sup>. Their electric resistivity data does not show a strong anomaly at  $T_{\text{N}}$ . This indicates that the carrier lifetime is influenced by magnetic ordering and the AFM SF only weakly and, thus, the system is in the perturbative regime, corresponding to very small  $r_{\text{sf}}$  in the plots of Fig. 4. Thus, the strong enhancement in the SH conductivity could be ascribed to the mechanisms developed in this work. The remaining question is which mechanism provides the main contribution to the SH effect in Cr, the side-jump mechanism or the skew-scattering mechanism. This will be answered when the SF fluctuation spectrum is carefully analyzed. Such analyses will also be helpful to understand and predict other AFM metallic systems for the SH effect.

At this moment, we are unaware of experimental reports of the SH effect in the vicinity of the AFM QCP. It might be worth investing the SH effect using  $\text{CeCu}_{6-x}\text{Au}_x$ <sup>47</sup> and other Ce compounds<sup>48</sup>. The temperature dependence of the SH conductivity might provide further insight into the nature of their QCP.

The SH effect near the FM critical temperature appears to depend on the material. Early studies on Ni-Pd alloys<sup>27</sup> reported that the temperature

dependence of the SH effect is analogous to that of the uniform second-order nonlinear susceptibility  $\chi_2$ , with a positive peak above  $T_C$  and a negative peak below  $T_C$ , thus showing the sign change across  $T_C$ . Such a behavior is qualitatively reproduced by a theoretical work by Gu et al.<sup>30</sup>, which adopted a static mean field approximation to the Kondo's model<sup>31</sup>. The current work, on the other hand, predicts that the SH effect of FM metals is maximized at  $T_C$ , while the same model is used as Gu et al. An experimental study by Ou et al. reported the sharp enhancement of the SH effect near  $T_C$  of Fe-Pt alloys<sup>28</sup>, the behavior resembles our prediction. A more recent experimental study by Wu et al. also reported a similar but weaker enhancement of the SH effect of Ni-Cu alloys<sup>29</sup>. How the SH effect depends on the material, changing sign or maximizing at  $T_C$ , remains an open question. One possible scenario is that the spin dynamics in Ni-Pd alloys is 'classical' in nature, while that in Fe-Pt and Ni-Cu alloys is more 'quantum', so that the theoretical analysis presented in this work is more relevant to the latter. Detailed experimental analysis on the spin dynamics of these FM metallic alloys using inelastic neutron scattering would settle this issue.

It is not obvious which SF generates the larger spin Hall effect, AFM or FM, because the detail of the materials property is involved. From the leading temperature dependence, the FM SF gives a stronger temperature dependence of the spin Hall conductivity when approaching  $T_C$  from higher temperature than the AFM fluctuation when approaching  $T_N$ . For FM metals, the spin Hall effect is expected to be replaced by the anomalous Hall effect below  $T_C$ , which is not the scope of the current study, while for AFM metals the spin Hall effect should persist down to low temperatures. Thus, both systems could be useful for the spintronic application depending on the temperature range.

To summarize, we developed the comprehensive theoretical description of the spin Hall effect in magnetic metallic systems due to the spin fluctuation. The special focus is paid to the antiferromagnetic spin fluctuation with nonzero Néel temperature  $T_N$  and  $T_N = 0$ , and the FM SF with nonzero Curie temperature  $T_C$ . In contrast to the spin Hall effect due to the ferromagnetic critical fluctuation, where the skew-scattering mechanism is one or two orders of magnitude stronger than the side-jump mechanism, the relative strength of the mechanisms could be altered depending on the detail of the spin-fluctuation spectrum and temperature. In particular, for antiferromagnetic metals, the skew-scattering mechanism becomes progressively dominant when approaching the magnetic transition temperature  $T_N$ , while the side-jump contribution becomes dominant by lowering temperature below  $T_N$ . The crossover from the skew scattering to the side jump also appears in a quantum critical system, where  $T_N$  is tuned to zero temperature. Aside from the absolute magnitude of the spin Hall conductivity, antiferromagnetic metals and ferromagnetic metals could be complementary in nature. This work thus provides an important component in antiferromagnetic spintronics<sup>49</sup>. Many magnetic metallic systems have been reported to show a variety of Hall effects, for example the anomalous Hall effect in  $\text{Fe}_3\text{GeTe}_2$ <sup>50</sup>, induced by the nontrivial band topology due to the orbital complexity, the spin-orbit coupling, as well as magnetic ordering. In the presence of such complexities, the predicted scaling law of the spin Hall effect could be modified, while the critical enhancement would not be entirely eliminated. Such an interplay will be an exciting research area, but left for future study.

## Data availability

The data that support the findings of this study are available from the corresponding author upon reasonable request.

Received: 15 August 2023; Accepted: 8 February 2024;

Published online: 19 March 2024

## References

- D'yakonov, M. I. & Perel, V. I. Possibility of orienting electron spins with current. *JETP Lett.* **13**, 467–469 (1971).
- D'yakonov, M. I. & Perel, V. I. Current-induced spin orientation of electrons in semiconductors. *Phys. Lett.* **35A**, 459–460 (1971).
- Hirsch, J. E. Spin Hall effect. *Phys. Rev. Lett.* **83**, 1834–1837 (1999).
- Saitoh, E., Ueda, M., Miyajima, H. & Tatara, G. Conversion of spin current into charge current at room temperature: inverse spin-Hall effect. *Appl. Phys. Lett.* **88**, 182509 (2006).
- Maekawa, S. Concepts in Spin Electronics (Oxford University Press, Oxford, U.K., 2006).
- Murakami, S. & Nagaosa, N. Spin Hall Effect. *Comprehensive Semiconductor Science and Technology* 1, Elsevier, 222–278 (2011).
- Sinova, J., Valenzuela, S. O., Wunderlich, J., Back, C. H. & Jungwirth, T. Spin Hall effects. *Rev. Mod. Phys.* **87**, 1213–1259 (2015).
- Nagaosa, N., Sinova, J., Onoda, S., MacDonald, A. H. & Ong, N. P. Anomalous Hall effect. *Rev. Mod. Phys.* **82**, 1539–1592 (2010).
- Sinova, J. et al. Universal Intrinsic Spin Hall Effect. *Phys. Rev. Lett.* **92**, 126603 (2004).
- Murakami, S., Nagaosa, N. & Zhang, S.-C. Spin-Hall Insulator. *Phys. Rev. Lett.* **93**, 156804 (2004).
- Smit, J. The spontaneous hall effect in ferromagnetics I. *Physica (Amsterdam)* **21**, 877–887 (1955).
- Smit, J. The spontaneous hall effect in ferromagnetics II. *Physica (Amsterdam)* **24**, 39–51 (1958).
- Berger, L. Side-jump mechanism for the hall effect of ferromagnets. *Phys. Rev. B* **2**, 4559–4566 (1970).
- Berger, L. Application of the side-jump model to the hall effect and nernst effect in ferromagnets. *Phys. Rev. B* **5**, 1862–1870 (1972).
- Crépieux, A. & Bruno, P. Theory of the anomalous Hall effect from the Kubo formula and the Dirac equation. *Phys. Rev. B* **64**, 014416 (2001).
- Tse, W.-K. & Das Sarma, S. Spin hall effect in doped semiconductor structures. *Phys. Rev. Lett.* **96**, 056601 (2006).
- Wang, L. et al. Giant room temperature interface spin hall and inverse spin hall effects. *Phys. Rev. Lett.* **116**, 196602 (2016).
- Gorini, C., Eckern, U. & Raimondi, R. Spin Hall effects due to phonon skew scattering. *Phys. Rev. Lett.* **115**, 076602 (2015).
- Karnad, G. V. et al. Evidence for phonon skew scattering in the spin Hall effect of platinum. *Phys. Rev. B* **97**, 100405(R) (2018).
- Xiao, C., Liu, Y., Yuan, Z., Yang, S. A. & Niu, Q. Temperature dependence of side-jump spin Hall conductivity. *Phys. Rev. B* **100**, 085425 (2019).
- Hoffmann, A. Spin hall effects in metals. *IEEE Trans. Magn.* **49**, 5172–5193 (2013).
- Okamoto, S., Egami, T. & Nagaosa, N. Critical spin fluctuation mechanism for the Spin Hall effect. *Phys. Rev. Lett.* **123**, 196603 (2019).
- Moriya, T. Spin Fluctuations in Itinerant Electron Magnetism, *Solid-State Sciences* **56** (Springer-Verlag, Berlin, 1985).
- Moriya, T. & Ueda, K. Spin fluctuations and high temperature superconductivity. *Adv. Phys.* **49**, 555–606 (2000).
- Ueda, K. & Moriya, T. Contribution of spin fluctuations to the electrical and thermal resistivities of weakly and nearly ferromagnetic metals. *J. Phys. Soc. Jpn* **39**, 605–615 (1975).
- Ueda, K. Electrical resistivity of antiferromagnetic metals. *J. Phys. Soc. Jpn* **43**, 1497–1508 (1975).
- Wei, D. H. et al. The spin Hall effect as a probe of nonlinear spin fluctuations. *Nat. Commun.* **3**, 1058 (2012).
- Ou, Y., Ralph, D. C. & Buhrman, R. A. Strong enhancement of the spin Hall effect by spin fluctuations near the curie point of  $\text{Fe}_x\text{Pt}_{1-x}$  alloys. *Phys. Rev. Lett.* **120**, 097203 (2018).
- Wu, P.-H. et al. Exploiting spin fluctuations for enhanced pure spin current. *Phys. Rev. Lett.* **128**, 227203 (2022).
- Gu, B., Ziman, T. & Maekawa, S. Theory of the spin Hall effect, and its inverse, in a ferromagnetic metal near the Curie temperature. *Phys. Rev. B* **86**, 241303(R) (2012).
- Kondo, J. Anomalous Hall effect and magnetoresistance of ferromagnetic metals. *Prog. Theor. Phys.* **27**, 772–792 (1962).

32. Du, C., Wang, H., Yang, F. & Hammel, P. C. Systematic variation of spin-orbit coupling with  $d$ -orbital filling: large inverse spin Hall effect in  $3d$  transition metals. *Phys. Rev. B* **90**, 140407(R) (2014).
  33. Qu, D., Huang, S. Y. & Chien, C. L. Inverse spin Hall effect in Cr: independence of antiferromagnetic ordering. *Phys. Rev. B* **92**, 020418(R) (2015).
  34. Fang, C. et al. Observation of the fluctuation spin hall effect in a low-resistivity antiferromagnet. *Nano Lett.* **23**, 11485 (2023).
  35. Anderson, P. W. Localized magnetic states in metals. *Phys. Rev.* **124**, 41–53 (1961).
  36. Kondo, J. Resistance minimum in dilute magnetic alloys. *Prog. Theor. Phys.* **32**, 37–49 (1964).
  37. Moriya, T. & Kawabata, A. Effect of spin fluctuations on itinerant electron ferromagnetism. *J. Phys. Soc. Jpn* **34**, 639–651 (1973).
  38. Moriya, T. & Kawabata, A. Effect of spin fluctuations on itinerant electron ferromagnetism. II. *J. Phys. Soc. Jpn* **35**, 669–676 (1973).
  39. Hertz, J. A. Quantum critical phenomena. *Phys. Rev. B* **14**, 1165–1184 (1976).
  40. Millis, A. J. Effect of a nonzero temperature on quantum critical points in itinerant fermion systems. *Phys. Rev. B* **48**, 7183–7196 (1993).
  41. Nagaosa, N. Quantum Field Theory in Strongly Correlated Electron Systems (Springer-Verlag, Berlin, 1999).
  42. Schrieffer, J. R., Wen, X. G. & Zhang, S. C. Dynamic spin fluctuations and the bag mechanism of high- $T_c$  superconductivity. *Phys. Rev. B* **39**, 11663–11679 (1989).
  43. Wölfle, P. & Ziman, T. Theory of record thermopower near a finite temperature magnetic phase transition in IrMn. *Phys. Rev. B* **104**, 054441 (2021).
  44. Baber, W. G. The contribution to the electrical resistance of metals from collisions between electrons. *Proc. R. Soc. A* **158**, 383–396 (1937).
  45. Bloch, F. Z. To the electrical resistance law at low temperatures. *Physik* **59**, 208–214 (1930).
  46. Ziman, J. M. Electrons and Phonons: The Theory of Transport Phenomena in Solids (Oxford, 1960).
  47. Löhneysen, H. V. Non-Fermi-liquid behaviour in the heavy-fermion system  $\text{CeCu}_{6-x}\text{Au}_x$ . *J. Phys. Condens. Matter* **8**, 9689–9706 (1996).
  48. Löhneysen, H. V., Rosch, A., Vojta, M. & Wölfle, P. Fermi-liquid instabilities at magnetic quantum phase transitions. *Rev. Mod. Phys.* **79**, 1015–1075 (2007).
  49. Baltz, V. et al. Antiferromagnetic spintronics. *Rev. Mod. Phys.* **90**, 015005 (2018).
  50. Kato, Y. D. et al. Optical anomalous Hall effect enhanced by flat bands in ferromagnetic van der Waals semimetal. *npj Quantum Mater.* **7**, 73 (2022).
- JPMJCR1874, Japan, and JSPS KAKENHI Grant number 18H03676. We thank Dr. Chi Fang, Prof. Yuan Lu, and Prof. Xiufeng Han for their stimulating discussions and for sharing their experimental data. Copyright notice: This manuscript has been authored by UT-Battelle, LLC under Contract No. DE-AC05-00OR22725 with the U.S. Department of Energy. The United States Government retains and the publisher, by accepting the article for publication, acknowledges that the United States Government retains a non-exclusive, paid-up, irrevocable, worldwide license to publish or reproduce the published form of this manuscript, or allow others to do so, for United States Government purposes. The Department of Energy will provide public access to these results of federally sponsored research in accordance with the DOE Public Access Plan (<http://energy.gov/downloads/doe-public-access-plan>).

### Author contributions

S.O. conceived the project and carried out calculations with input from N.N. Both authors contributed to the writing of the manuscript.

### Competing interests

The authors declare no competing interests.

### Additional information

**Supplementary information** The online version contains supplementary material available at <https://doi.org/10.1038/s41535-024-00631-9>.

**Correspondence** and requests for materials should be addressed to Satoshi Okamoto.

**Reprints and permissions information** is available at <http://www.nature.com/reprints>

**Publisher's note** Springer Nature remains neutral with regard to jurisdictional claims in published maps and institutional affiliations.

**Open Access** This article is licensed under a Creative Commons Attribution 4.0 International License, which permits use, sharing, adaptation, distribution and reproduction in any medium or format, as long as you give appropriate credit to the original author(s) and the source, provide a link to the Creative Commons licence, and indicate if changes were made. The images or other third party material in this article are included in the article's Creative Commons licence, unless indicated otherwise in a credit line to the material. If material is not included in the article's Creative Commons licence and your intended use is not permitted by statutory regulation or exceeds the permitted use, you will need to obtain permission directly from the copyright holder. To view a copy of this licence, visit <http://creativecommons.org/licenses/by/4.0/>.

© UT-Battelle, LLC and Naoto Nagaosa 2024

### Acknowledgements

The research by S.O. was supported by the U.S. Department of Energy, Office of Science, Basic Energy Sciences, Materials Sciences and Engineering Division. N.N. was supported by JST CREST Grant Number